Effect of Fe ion beam irradiation on structural, surface, optical, and electrical properties of ZnO thin films prepared by radio frequency sputtering

M. F. Khan [a,d], K. Siraj [a], S. Majeed [a], M. I. Khan [b,*], A. Sattar [c], H. Mustafa [c],
J. Raisanen [d], S. Hayat [b], M. Atif [e]
[a] *Laser and Optronics Centre, Department of Physics, University of Engineering and Technology, Lahore, Pakistan*
[b] *Department of Physics, The University of Lahore, 53700, Pakistan*
[c] *Department of Physics, Comsats Institute of Information Technology, Lahore, Pakistan*
[d] *Department of Physics, Division of Materials Physics, University of Helsinki, Finland*
[e] *Department of Physics and Astronomy, College of Science, King Saud University, P O Box 2455, Riyadh 11451, Saudi Arabia*

In this work, ZnO thin films were exposed to 80 keV Fe^{+1} ions at different fluences (1 x 10^{13}, 1 x 10^{14}, 5 x 10^{14}, 1 x 10^{15} ions/cm^2). With the help of X-ray diffraction (XRD), scanning electron microscopy (SEM), spectroscopic ellipsometry (SE), and the four-point probe technique, we were able to measure the structural and surface morphology, optical, and electrical properties of both untreated and irradiated ZnO thin films. X-ray diffraction research showed that crystallite size was diminished from its pristine level with the fluence of 1 x 10^{13} ions/cm^2, but that crystallite size increased along with the ion fluence, resulting in higher levels of crystallinity in the thin films. SEM images of a ZnO thin film exposed at the fluence of 5 x 10^{14} ions/cm^2 revealed acicular patterns on its surface. The electrical resistivity of ZnO thin film decreases as the fluence of ion increases. Consistency between the findings supports the idea that the observed behavior is due to the confined heating effect generated by ion irradiation of the thin films.

1. Introduction

Thin films of ZnO are gaining a lot of interest due to their broadband gap of 3.37 eV and significant exciton binding energy of 60 meV. At ambient temperature, it behaves as a semiconductor belonging to the II-VI family. No thin films are of great interest because to their outstanding magnetic, physical, and optoelectronic properties[1].ZnO thin films have generated a great deal of concern in application areas including light-emitting diodes, chemical sensors, solar cells, interfacial acoustic wave gadgets, optoelectronic technologies, and transparent conductive electrodes[2].

Several methods, including thermal sputtering, chemical vapor deposition (CVD), pulsed laser deposition (PLD), spray pyrolysis, molecular beam epitaxy (MBE), and radio frequency (RF) sputtering, can be used to create ZnO thin films[3]. RF sputtering was one of the methods of deposition, and it offered many notable advantages over the other methods, including a high deposition rate, an easy way to adjust the composition, and substrate homogeneity. Doping ZnO with a variety of anions and cations is the method that is the most successful in modifying or changing the morphological, electric, magnetic, and optical properties of the material. Doping the

---

ZnO thin films with the ions (for example Fe, Ni, Ag, and Cr) using ion irradiation is an efficient approach [4].

Many academic researchers have studied mostly on impacts of the bombardment of ions on thin films of ZnO. Ham et al. revealed the incorporation of hydrogen ions with energies of 200 keV and fluences of 10^{13} ions/cm^2 on ZnO thin films which increases both the refractive index and the energy band gap[5]. Hydrogen shallow donors or point defects were introduced into the material rather than damaged because of the increased energy of the optical band gap caused by proton implantation. Irradiation of an argon ion beam at 150 keV was used by Krishna et al. to produce regular nanostructures on ZnO thick films measuring 400 nm in thickness. Guner et al. investigated that the fluence increased from 0.25×10^{17} ion/cm^2 to 2×10^{17} ion/cm^2 when Co^{+1} ions were implanted into ZnO thin films at an energy of 40 keV. Increases in the concentration of Co^{+1} ions improved the electrical conductivity of the thin film while decreasing its crystallinity. In addition to this, the ferromagnetic characteristics of the Co-ZnO thin film were shown even at ambient temperature[6]. Sagaguchie et al. show the effects of annealing ZnO thin films with 170 keV indium ions inserted after conducting their research. Kuchyev and colleagues investigated structural flaws in ZnO that had been subjected to bombardment with ions of Si and Au with energies of 60 keV and 300 keV respectively. Y.H.Xue et al demonstrated that the magnetic, structural, and optical characteristics of the ZnO thin films were altered in a many ways when 120 keV Fe ions at a fluence of 5×10^{16} ions/cm^2 and 20 keV C ions at a fluence of 3×10^{15} ions/cm^2 were implanted into ZnO thin films. A. Kumar and colleagues discovered that the magnetic, structural, and optical characteristics of ZnO thin films may be altered by implanting Fe^{10+} ions with energies of 300 keV at fluences varying from 3×10^{15} to 1×10^{17} ions/cm^2 on the surface of the films[7-9].

Lattice damage, in the form of vacancies, interstitials, or even volume defects, is a predictable and unavoidable side effect of ion implantation. Material faults may influence the physical, electrical, and optical properties as well as structural morphology[10]. Because of this, it is very necessary to explore the implantation-induced changes in the physical characteristics of thin films which will clarify the operation and fabrication of metal ions irradiated base ZnO devices[11].

There are two primary justifications for opting to use Fe as the most suitable and workable dopant. To begin, the effective ionic radii of iron, which are 0.64 angstroms, are comparable to those of zinc, which are 0.74 angstroms. This similarity helps to control and, to some degree, prevent distortion of the crystal structure in Fe-doped zinc oxide. Second, the significance that the chemical state of the Fe ions plays in the modification of the energy band is significant. Zn ions might be replaced by Fe ions, which would result in the introduction of certain impurity levels and the enrichment of the energy level structure. Herein, ZnO thin films were prepared by RF sputtering and bombarded with 80 keV Fe^{1+} ions at different fluences showing the formation of nanostructures and their effect on changing the optical and electrical properties of ZnO thin films.

2. Experimental section

The experimental phase consists of two parts: the first part involves the deposition of a ZnO thin film, and the second part is the irradiation of ions on ZnO thin films. The first thing that was done was to use RF Sputtering to create five similar thin films on a glass substrate of (10mm ×10 mm×1mm). During the sputtering procedure, a pure ZnO target that had been commercially sintered and measured 3 millimeters in thickness and 3 inches in diameter was employed. Cleaning of glass substrates was done with a solution of mild soap before being rinsed extensively in DI water and then in boiling water before deposition process began. In last, substrates were cleaned in ultrasonic bath with ethanol for fifteen minutes. Deposition was carried out at a constant biasing voltage of 945 V DC for 30 minutes while the pressure was kept at 3×10^{-3} Torr. Ar flow rate was kept constant at 50 standard cubic centimeters per minute. The thickness of every single layer that was deposited was 80 ± 10 nm.

The second phase included implanting 80 keV Fe$^+$ ions into thin ZnO sheets using a Pelletron tandem accelerator [29]. The implantation procedure was completed under high vacuum (10^{-6} Torr) at room temperature. To serve as a reference, one ZnO thin film was retained in perfect condition. The beam current was maintained at 15, 40, 40, and 50 nAcm^{-2} for the fluences of 1×10^{13},

$1x10^{14}$, $5x10^{14}$, and $1x10^{15}$ ions/cm^2, respectively, throughout the irradiation. To prevent the channeling effect, all of the samples were slanted by 5 degrees and grounded electrically throughout the radiation process.

A range of 37.6 nm and drifting of 16.3 nm was calculated using SRIM 2010 [30]. It is found that the nuclear stopping power is 1.53×10^2 eV, whereas the electronic stopping power is 1.988×10^1 eV/. This experiment proves ZnO thin films of an average thickness 80 nm may withstand implantation rather than transmission of incoming ions. Blocking these ions in films allows the Zn^{+2} ions in the ZnO matrix to fill the void. The pure and irradiated ZnO thin films were characterized using several procedures. The structure morphology change was analyzed using an XRD (PANAlyticalX'Pert Powder) and CuK (1.5405) radiations in the 2Ɵ range of 20 to 80°. Using SEM (S4800), the surface morphology for pure and ionized thin films was analyzed. Transmission-mode spectroscopic ellipsometry was used to investigate the optical characteristics (JA Woolam Co Ellipsometer-M2000). Using a four-probe method, the electrical characteristics were determined.

3. Results and discussion

3.1. Structural analysis

Figure 1a displays the XRD spectra of both undamaged ZnO thin films and films that were exposed to 80 keV, $1x10^{13}$, $1x10^{14}$, $5x10^{14}$, and $1x10^{15}$ ions/cm^2 of Fe^{+1} ions. The peak is visible at 2 34.34° for all thin films that map to the ZnO (002) plane[12]. Irradiation removes peaks that correspond to impure phases. According to the results, the c-axis (002) plane is the sole direction in which the ZnO granules are firmly orientated. Nanocrystalline has a hexagonal quartzite structure, all ZnO thin films exhibit preferred (002) growth[13]. Table 1 and the equations (2.2-2.4) therein can be used to determine crystallographic characteristics such as d-spacing, average crystallite size, lattice parameters, dislocation density, and microscopic strain. Figure 1b depicts the relationship between the ion fluence and the crystallite size[14]. When the fluence is at its highest, the average crystalline size of ZnO thin films subjected to Fe^{+1} ion radiation decreases. It demonstrates how the ion beam has a detrimental effect on the grain formation of thin films of ZnO. Since much of the Fe+^{1} ions are now located in sites of Zn, no diffraction peak in can be ascribed to Fe-related secondary phases. Due to the high energy of the incoming ions, films as thin as 80 nm were successfully implanted. Dislocation density and lattice strain increase with temperature. Smaller crystals are the result of more dislocations, which in turn is generated by more prominent grain boundaries[15]. Lattice strain increases because of ion exposure in ZnO thin films (at the fluences of $1x10^{13}$, $1x10^{14}$, $5x10^{14}$, and $1x10^{15}$ ions/cm^2). This arises from the conflict between the ionic radii of the dopant Fe (0.62) and the host material Zn (0.74)[16].
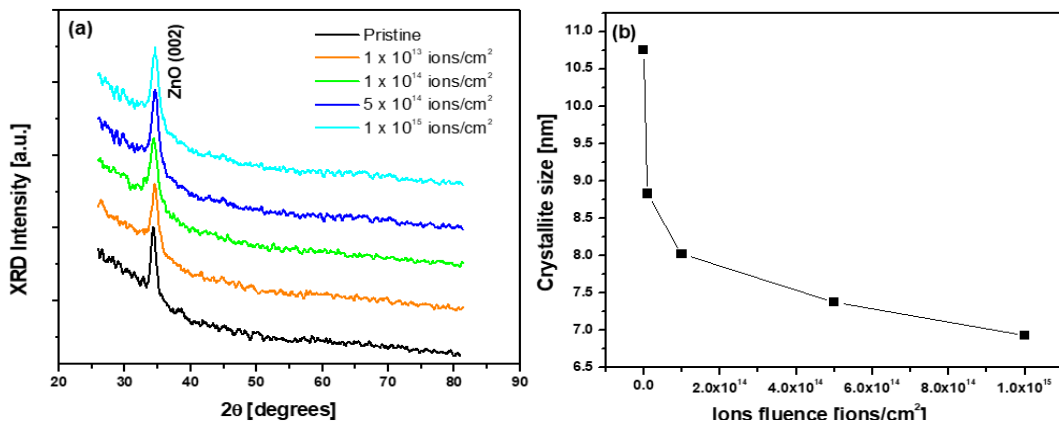

Fig. 1. (a) XRD spectra of untreated and ion-irradiated ZnO thin films. (b) Variation in crystallite size with fluence of ions.

Table 1. Comparison of untreated and ion irradiated ZnO thin films with respect to position of XRD peak, crystallite size, lattice parameter, dislocation density, and micro strains.

Ions fluence (Ions /cm^2)	2θ (Degree)	d-spacing (Å)	Lattice Parameters (Å)	Crystallite Size $D(nm)=\frac{k\lambda}{\beta\cos\theta}$	Dislocation Density (nm)$^{-2}$ $\frac{1}{D^2}$	Micro Strain $e=\frac{\beta\cos\theta}{4}$
Pristine	34.36	2.6099	5.210	10.75	8.65 ×10^{-3}	3.22 ×10^{-3}
1 × 10^{13}	34.64	2.5895	5.179	8.83	12.82×10^{-3}	3.92×10^{-3}
1 × 10^{14}	34.46	2.6025	5.205	8.02	15.55×10^{-3}	4.32×10^{-3}
5 × 10^{14}	34.70	2.5851	5.170	7.38	18.36×10^{-3}	4.70 ×10^{-3}
1 × 10^{15}	34.64	2.5895	5.179	6.93	20.82×10^{-3}	5.00×10^{-3}

3.2. Morphology of surface

Micrographs of ZnO thin films acquired with a SEM before and after being irradiated 1x10^{13}, 1x10^{14}, 5x10^{14}, and 1x10^{15} ions/cm^{2}of Fe^{+1}ions at 80 keV are shown in Figure 2(a-e).When subjected to different concentrations of Fe^{+1} ions, each of these micrographs reveals high-quality films that experience discernible changes in their morphology because of the treatment[17]. The pure ZnO thin film has a surface that is devoid of cracks and has a smooth texture (see Fig. 2(a)). Nanoparticles on the top of a ZnO thin film begin to clump together and take on a leaf-like shape when exposed to radiation with a fluence of 1 x 10^{13} ions/cm2 (Fig. 2b). On the top of the thin film, there are micro leaves with the shape of circular pyramids and pyramids of varied sizes. When micro-sized circular and pyramidal structures agglomerate at fluences of 1 × 10^{14} and 5 × 10^{14} ions /cm^2, longer leaf structures are generated[18]. These fluences are used to measure ions (Fig. 2c-d).
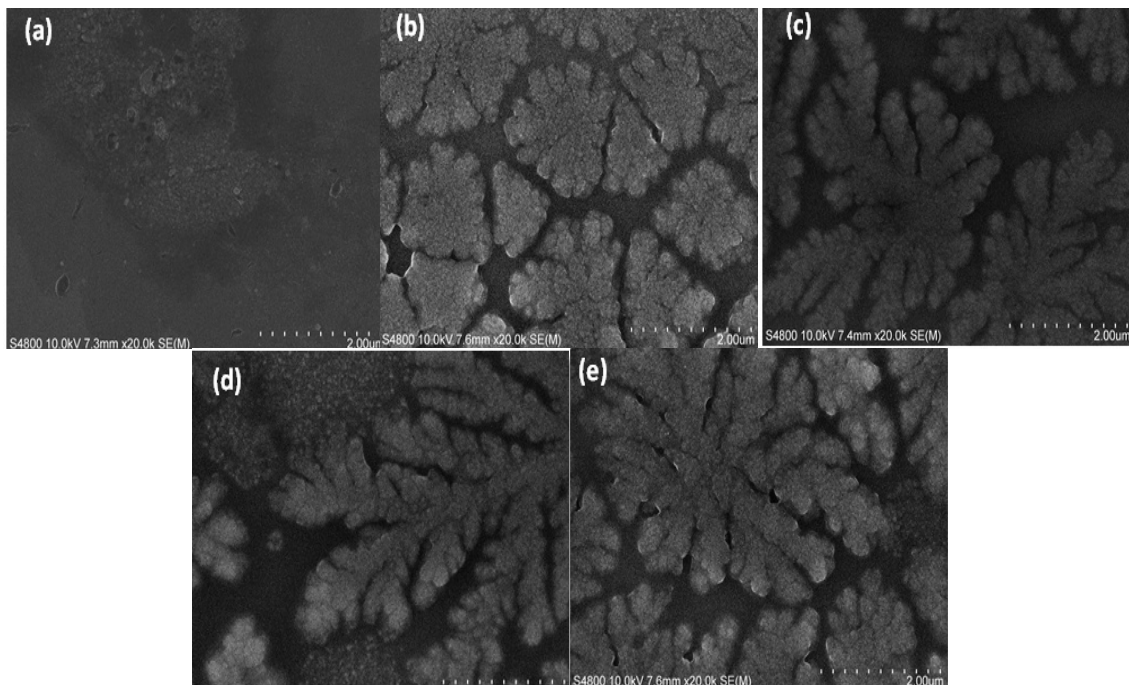

Fig. 2. Images obtained from scanning electron microscopy of ZnO before and after irradiation with Fe^{+1} ions at varying fluences. (a) sterile; (b) 1 × 10^{13} ion/cm^2(c) 1 × 10^{14} ion/cm^2; (d) 5 × 10^{14} ion/cm^2 and (e) 1 × 10^{15} ion/cm^2.

When the number of ions per square centimeter is raised to 1 x 10^{15} ions/cm^2, the tiny leaves already on the surface of the ZnO thin film get bigger (Fig. 2e). As the volume of water passing through the channel increases, fractured-shape formations consisting of several fine arms begin to take shape. This is due to the influence that the impurity Fe ion has on the surface of film. The nucleation density of ZnO is raised by the addition of Fe ions to the material. Surface morphology analysis of irradiated thin films provides qualitative evidence of enhanced surface roughness compared to untreated films[19].

3.3. AFM analysis

Using tapping mode atomic force microscopy (AFM), we compare the surface profile of ZnO thin films that have not been modified to those that have been exposed to Fe^{+1} ions through irradiation. Figure 3 (a-e) shows the two-dimensional and three-dimensional profiles of thin films made of pure ZnO and ZnO that has been irradiated with Fe^{+1}. The area of scan is 2μm × 2μm. A perfect film will have an RMS roughness of around 1.16 nanometers. The surface of the thin film contains particles ranging in size from 30 to 70 nanometers[20]. Particle roughness averages 2.06 nm and particle size ranges from 50 to 300 nm at low fluence (1 x 10^{13} ions/cm^2). Nanocluster formation results in an increase in the size of the produced particle. When the rms roughness is raised to 2.39 nm and the ion fluence is raised to 1 x 10^{14} ions/cm2, the allocation of particle on the surface shifts to be between 40 and 150 nm. Nano-crystallites can only form in the presence of this temperature and pressure, and they do so alongside bigger grains. When the fluence is increased to 5 x 1014 ions/cm^2, particles that range in size from 50 nm to 180 nm are produced. This results in a significant reduction in the roughness of the surface, which falls to a value of 2.32 nm. The energy that is deposited during the ion bombardment at this fluence causes the nanostructures to shrink, which indicates that the average particle size and roughness are decreased. The roughness of the surface rose to 3.65 nm when it was subjected to the maximal fluence that was applied (51014 ions/cm^2), and the particle size on the surface ranged from 40 to 200 nm. This finding provides evidence that the nanostructures were changed into gigantic submicron sizes[1, 21].
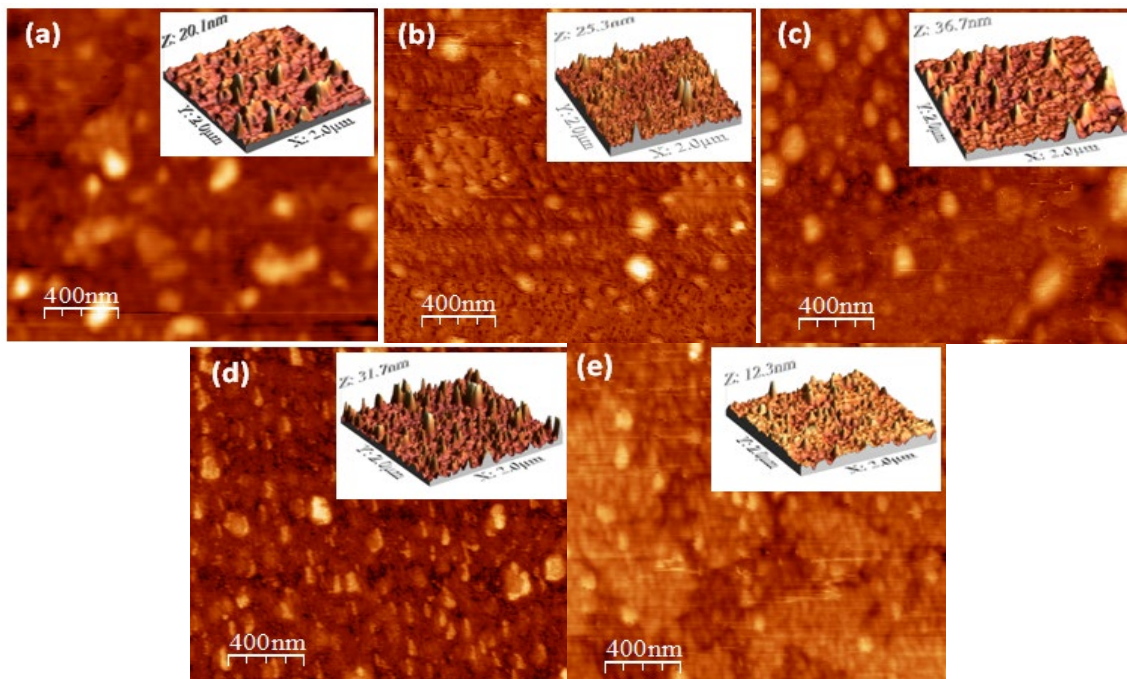

Fig. 3. Various ion fluences were used to get two- and three-dimensional pictures using atomic force microscopy of untreated, and ion irradiated thin films of ZNO(a) sterile; (b) 1× 10^{13} ion/cm^2 (c) 1× 10^{14} ion/cm^2; (d) 5 × 10^{14} ion/cm^2 and (e) 1 × 10^{15} ion/cm^2.

3.4. Optical analysis

Figure 4 (a,b) monitor the fluctuations in optical constants such as refractive index "n" and extinction coefficient "k" within the range of wavelengths from 383 nm to 900 nm. Refractive index progressively lowers from 383 to 900 nm in both untreated and Fe^{+1} ion irradiated thin films of ZnO at various fluences i.e., $1x10^{13}$, $1x10^{14}$, $5x10^{14}$, and $1x10^{15}$ ions/cm^2as shown in Figure 4a. All thin films have a refractive index that falls between 2.28 and 2.38 when measured at a wavelength of 383 nm; when measured at a wavelength of 900 nm, the refractive index ranges from 2.02 to 206[22, 23]. Across the whole visible spectrum, all ZnO thin films treated with ion irradiation have a lesser refractive index than untreated thin films. This is true for all wavelengths of visible light. The refractive index curve undergoes variations of an unanticipated nature as the ion fluence increases. ZnO thin films are transparent regardless of whether they have been treated with Fe^{+1} ions (Fig. 4b). The pristine and Fe^{+1} irradiated ZnO thin films display maximum values of 0.21 and 0.35 for the extinction coefficient when measured at a wavelength of about 383nm and fluences of $1x10^{13}$, $1x10^{14}$, $5x10^{14}$, and $1x10^{15}$ ions/cm^2, respectively[24]. When the wavelength is made longer, the extinction coefficient becomes less significant[25]. All ZnO thin films, both unmodified and ion-irradiated, are transparent between 600 and 900 nm, with a band edge at 600 nm and an extinction coefficient that stabilizes as the wavelength moves from the visible to the infrared ranges. The extinction coefficient curves undergo a nonlinear transformation whenever the ion fluence is increased. The energy of the optical band gaps may be approximated with the help of Tauc's relation 3.1, which can be found here[26].
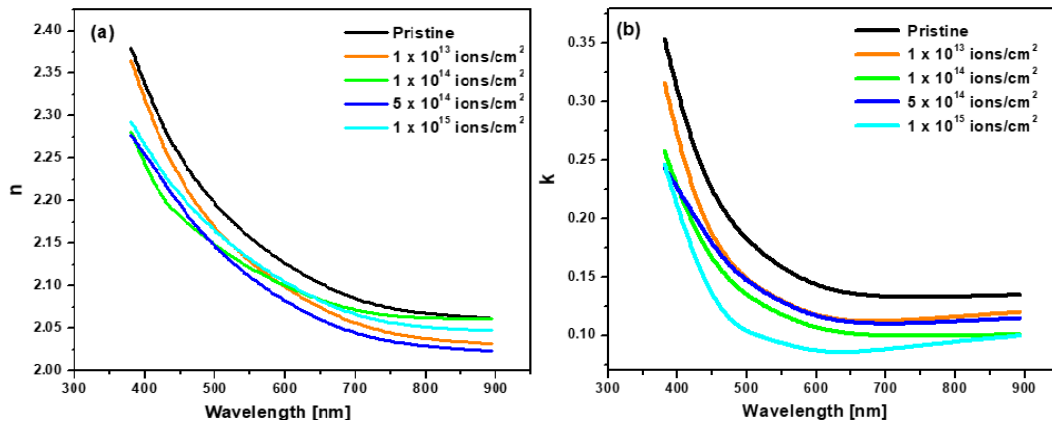

Fig. 4. Variation in (a) refractive index "n" and (b) extinction coefficient "k" with a wavelength in untreated and ion-irradiated ZnO thin films.

Figure 5 (a-e) displays the graphs plotted between values of $(\alpha h\nu)^2$and hν of untreated and ion-irradiated ZnO thin films. Figure 5a represents the estimate of the band gap energy that is obtained by examining the Tauc's curves of untreated and ion-irradiated thin films of zinc oxide as a function of ion fluence (E_g). The value of E_g that was measured, which was 3.37 eV, is a little bit less 3.10 eV that was discovered in pristine ZnO thin film[27]. The ZnO thin film has a greater number of naturally occurring defects or oxygen vacancies. When the fluence of ions is boosted to 1×10^{15} ion/cm^2, E_g falls to the value of 2.6 eV from 3.10 eV (for a clean layer). The steepness of the Eg curves as a parameter of fluence is strongly correlated with the presence of crystalline thin layers. This is because crystalline thin films are made up of very few atoms. The disparity in energy levels between the various bands is decreasing for two primary reasons[28]. The presence of Fe ions may create defect levels just below the conduction band. Another possible cause is the sp-d exchange between the ZnO band electrons and the Fe band d-electrons. This is quite likely to be the factor that is generating the observable phenomena[29].
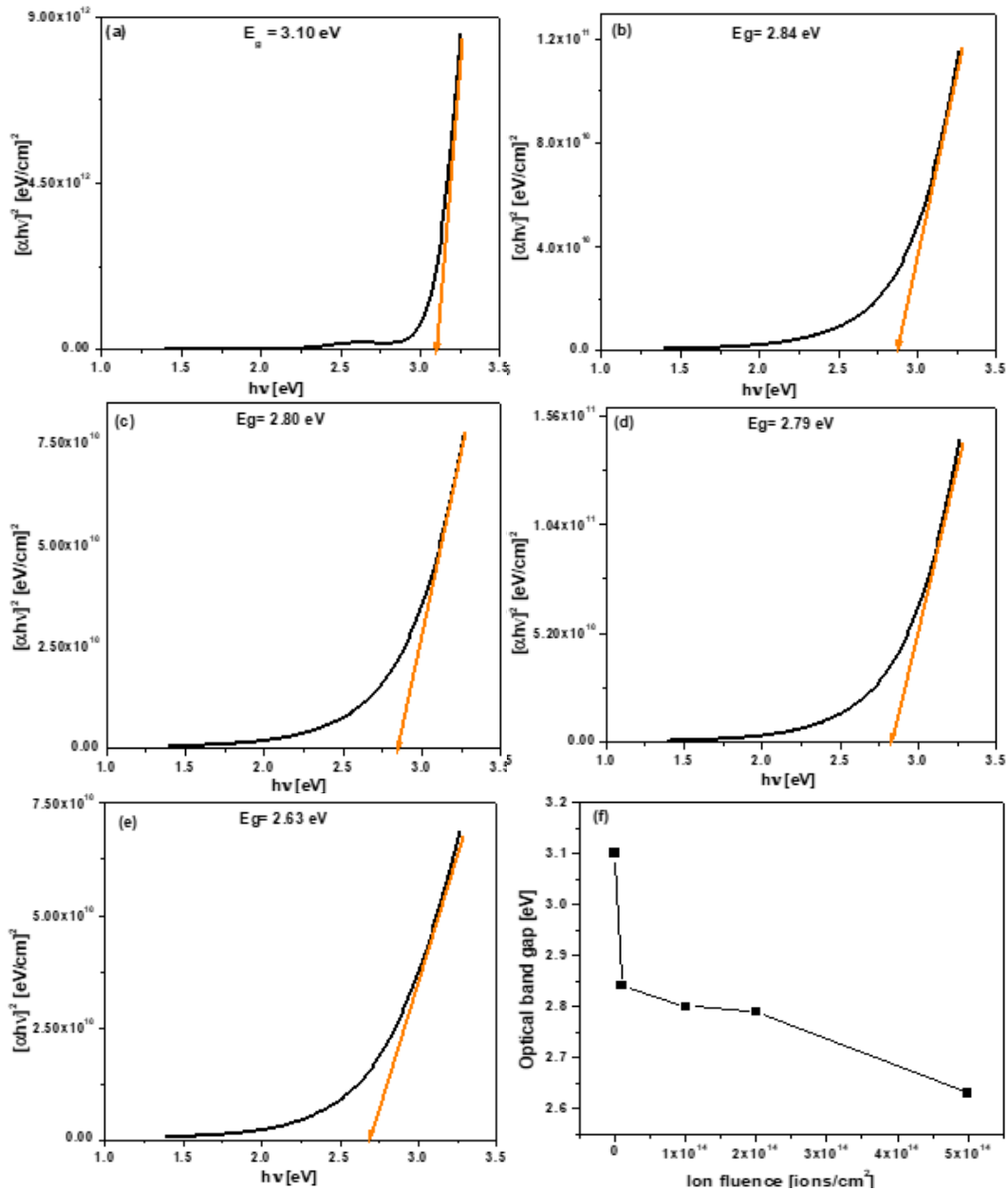
Fig. 5. Graphs plotted between values of $(\alpha h v)^2$ and hvcurves of untreated and ion irradiated ZnO thin films. (a) untreated ZnO thin films, (b) 1×10^{13} ion/cm^2 (c) 1×10^{14} ion/cm^2; (d) 5×10^{14} ion/cm^2 and (e) 1×10^{15} ion/cm^2.

3.5. Electrical resistivity

Figure 6 illustrates the differences in electrical resistivity that occur between un-irradiated ZnO thin films and those that have been irradiated with Fe^{+1} ions. The resistivity of ZnO thin films decreased from its starting value of 6.5×10^{-2} Ω/cm (untreated) when the fluence of the ions per square centimeter is 1×10^{15} ions/cm^2, to the lowest of 2.35×10^{-6} Ω-cm[30]. The decrease in electrical resistivity may be attributed to increased carrier concentration as well as electron displacement from Fe^{+1} donors at Zn^{+2} substitutional sites in the films. The incoming ions may have generated some structural defects and oxygen vacancies in the thin layer, which would explain the observed decline in electrical resistivity[31].
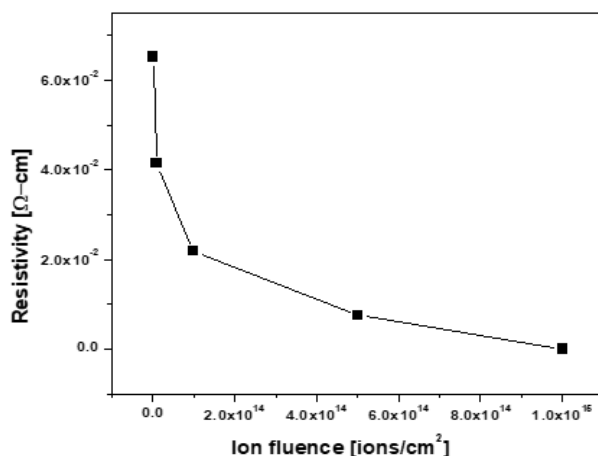
Fig. 6. Trend of variation in electrical resistivity untreated and ion irradiated ZnO thin films at different ion fluence.

4. Conclusion

We have examined the modifications in structure, morphology, electrical, and optical behavior of ZnO thin films with and without the Fe^{+1} ion irradiation. The crystallinity of ZnO thin films improved after ion irradiation. Surface roughness and electrical resistivity of ZnO thin films decrease. The refractive index and extinction coefficient also decrease with an increase in wavelength. In ZnO thin films, the Fe^{+1} ion irradiation caused a local annealing effect, as well as oxygen vacancies, and produced defects in the structure. The electrical resistivity of ion-irradiated ZnO thin films exponentially decreases due to Fe^{+1} ions irradiation, which increases carrier concentration as well as electron displacement from Fe^{+1} donors at Zn^{+2} substitutional sites in the ZnO thing films. Structural defects and oxygen vacancies created by Fe^{+1} ion irradiation may also be a cause of a decrease in electrical resistivity.

Acknowledgement

References

[1] Dejam, L., M. Ilkhani, Optical and Quantum Electronics, 2024. 56(3): p. 444;
https://doi.org/10.1007/s11082-023-06071-2

[2] Lekoui, F., et al., Optical Materials, 2024. 150: p. 115151;
https://doi.org/10.1016/j.optmat.2024.115151

[3] Godiwal, R., et al., Optical Materials, 2024. 148: p. 114919;
https://doi.org/10.1016/j.optmat.2024.114919

[4] Krysova, H., et al., Journal of Solid State Electrochemistry, 2024: p. 1-16;
https://doi.org/10.1007/s10008-023-05766-6

[5] Krishna, S.B.N., et al., Journal of Materials Chemistry B, 2024;
https://doi.org/10.1039/D4TB00184B

[6] Ozel, K., Sensors and Actuators A: Physical, 2024. 366: p. 114953;
https://doi.org/10.1016/j.sna.2023.114953

[7] Mrabet, C., et al., Materials Science and Engineering: B, 2024. 300: p. 117130;
https://doi.org/10.1016/j.mseb.2023.117130

[8] Le, M.P., et al., Applied Surface Science, 2024: p. 159785;
https://doi.org/10.1016/j.apsusc.2024.159785

[9] Bolli, E., et al., Crystals, 2024. 14(1): p. 90; https://doi.org/10.3390/cryst14010090

[10] Prieto, P., et al., Interactions, 2024. 245(1): p. 53; https://doi.org/10.1007/s10751-024-01897-y

[11] Chaudhary, S., et al., Microscopy Research and Technique, 2024;
https://doi.org/10.1002/jemt.24598

[12] Sathya, M., et al., The European Physical Journal Plus, 2023. 138(1): p. 1-12;
https://doi.org/10.1140/epjp/s13360-023-03667-1

[13] Dejam, L., et al., Results in Physics, 2023. 44: p. 106209;
https://doi.org/10.1016/j.rinp.2023.106209

[14] Khan, M., et al., RSC advances, 2024. 14(8): p. 5440-5448;
https://doi.org/10.1039/D3RA08965G

[15] Khan, M.I., et al., CrystEngComm, 2024; https://doi.org/10.1039/D4CE00300D

[16] Aboud, A.A., et al., Physica Scripta, 2023. 98(9): p. 095958;
https://doi.org/10.1088/1402-4896/acf167

[17] Amri, A., et al., Results in Optics, 2023. 11: p. 100426;
https://doi.org/10.1016/j.rio.2023.100426

[18] López-Suárez, A., et al., Journal of Materials Science: Materials in Electronics, 2020.
31(10): p. 7389-7397; https://doi.org/10.1007/s10854-019-02830-8

[19] Fan, Q., et al., Journal of Alloys and Compounds, 2020. 829: p. 154483;
https://doi.org/10.1016/j.jallcom.2020.154483

[20] Bancheva-Koleva, P., et al., Materials, 2024. 17(9): p. 2164;
https://doi.org/10.3390/ma17092164

[21] Abdallah, B., et al., Acta Microscopica, 2023. 32(1).

[22] Khan, M., et al., Physica B: Condensed Matter, 2024. 678: p. 415758;
https://doi.org/10.1016/j.physb.2024.415758

[23] Kim, D., J.-Y. Leem, Scientific reports, 2021. 11(1): p. 382;
https://doi.org/10.1038/s41598-020-79849-z

[24] Khan, M., et al., New Journal of Chemistry, 2024; https://doi.org/10.1039/D4NJ00681J

[25] Su, L., W. Ouyang, X. Fang, Journal of Semiconductors, 2021. 42(5): p. 052301;
https://doi.org/10.1088/1674-4926/42/5/052301

[26] Khan, M., et al., Physical Chemistry Chemical Physics, 2024. 26(5): p. 4166-4173;
https://doi.org/10.1039/D3CP05339C

[27] Khan, M., et al., Physical Chemistry Chemical Physics, 2024;
https://doi.org/10.1039/D3CP06299F

[28] Almutairi, B.S., et al., Optical Materials, 2024. 152: p. 115415;
https://doi.org/10.1016/j.optmat.2024.115415

[29] Yergaliuly, G., et al., Scientific reports, 2022. 12(1): p. 851;
https://doi.org/10.1038/s41598-022-04782-2

[30] Mujtaba, A., et al., Journal of Materials Research and Technology, 2023. 23: p. 4538-4550;
https://doi.org/10.1016/j.jmrt.2023.02.038

[31] Nobre, J.H.F., et al., Applied Physics A, 2023. 129(3): p. 203;
https://doi.org/10.1007/s00339-023-06490-8